# Treating different bonding situations: Revisiting Au-Cu alloys using the random phase approximation

Niraj K. Nepal,[1,*] Santosh Adhikari,[1] Jefferson E. Bates,[2] and Adrienn Ruzsinszky[1]

[1]*Department of Physics, Temple University, Philadelphia, Pennsylvania 19122, USA*
[2]*A.R. Smith Department of Chemistry and Fermentation Sciences, Appalachian State University, Boone, North Carolina 28607, USA*

The ground-state equilibrium properties of copper-gold alloys have been explored with the state-of-the-art random phase approximation (RPA). Our estimated lattice constants agree with the experiment within a mean absolute percentage error of 1.4 percent. Semilocal functionals, such as the generalized gradient approximation (GGA) of Perdew, Burke, and Ernzerhof (PBE) and the strongly constrained and appropriately normed (SCAN) functional, fail to provide accurate bulk moduli, which indicates their inability to describe the system in a stretched or compressed state with respect to the equilibrium geometry. The PBE, PBE revised for solids, and revised Tao-Perdew-Staroverov-Scuseria functionals by Perdew *et al.* predict too-low formation energies, while the SCAN slightly overestimates it. The inclusion of thermal correction or the long-range dispersion provides a negligible contribution to the formation energies estimated with semilocal density functional theory. The spin-orbit coupling improves the formation energies of PBE only by 7–8 meV, while it intensifies the overestimation of SCAN. We found that the nonlocality present in RPA is able to describe the transition between two delocalized electron densities (bulk elemental constituents to crystallized alloys), as required to provide accurate formation energies without any further corrections. Based on our results, we conclude that it is difficult to find a universal density functional which can give accurate results for a wide range of properties of intermetallic alloys. However, RPA can capture different bonding situations, often better than other density functionals. It gives accurate results for a wide range of ground-state properties for the alloys, generated from metals with completely filled $d$ shells.

## I. INTRODUCTION

Intermetallic alloys, the mixture of two or more metals in a solid form, manifest a defined stoichiometry and an ordered crystal structure [1]. The brittleness and high melting point with various electronic and magnetic properties of these solid compounds make them significantly useful in industrial applications. The heat of formation or formation energy of an alloy is the difference between the total binding energy of the system and its pure constituents, and its accurate prediction is extremely important in alloy theory. It governs the stability of the alloys with different compositions at different temperatures and pressures [1,2].

Density functional theory (DFT) is a robust electronic structure method, applicable across numerous fields of science. Various forms of the approximation to the exchange-correlation (xc) energy, a key but unknown quantity in DFT, afford different levels of accuracy and computational efficiency. These different forms constitute the different rungs of Perdew's Jacob's ladder [3]. The local density approximation (LDA) [4] and generalized gradient approximations (GGA) such as Perdew-Burke-Ernzerhof (PBE) [5], AM05 by Armiento and Mattsson [6], and PBE revised for solids

(PBEsol) [7], though being highly accurate and efficient in many cases, often fail to provide an accurate description of the properties which require either self-interaction correction, at least a fraction of exact exchange, or an adequate description of many-body correlation [8]. Meta-GGAs such as TPSS [9] by Tao, Perdew, Staroverov, and Scuseria, the made-simple (MS) family [10,11], and strongly constrained and appropriately normed (SCAN) [12] functionals provide significant improvement over LDA and GGAs, with the inclusion of kinetic-energy density [$\tau(\mathbf{r})$] as an ingredient in addition to the density [$n(\mathbf{r})$] and its gradient [$\nabla n(\mathbf{r})$]. However, regarding the formation energy of intermetallic alloys, semilocal functionals have a mixed performance [13–15]. To estimate an accurate formation energy, a functional should not only provide reliable energetics of an alloy but also simultaneously of its constituent elements. However, most semilocal functionals fail in that regard, leading to inaccurate predictions of the formation energy [16].

At high temperature, copper and gold form a continuous solid solution, while they crystallize to form Au-Cu superlattices at lower temperature [17]. The Au-Cu systems, $AuCu_3$ (or $Au_{0.25}Cu_{0.75}$), AuCu (or $Au_{0.5}Cu_{0.5}$), and $CuAu_3$ (or $Au_{0.75}Cu_{0.25}$), are the paradigms of intermetallic alloys, and have been extensively studied with semilocal as well as nonlocal DFT methods [14–16]. Experimentally, the fully ordered $AuCu_3$ and $CuAu_3$ stabilize in the $L1_2$ phase, while

*niraj.nepal@temple.edu

the ordered AuCu prefers the L1$_0$ phase at $T = 0$ K [1]. In addition to the distorted face-centered-cubic (fcc) phase for AuCu (L1$_0$), we also have explored its fcc phase. Previous work clearly established that LDA could not predict the ground state of CuAu$_3$ as the L1$_2$ phase and also significantly underestimates the formation energies of all the Au-Cu alloys [15]. Similar to LDA, PBE also predicts CuAu$_2$ as the stable phase and CuAu$_3$ as the unstable one [14]. On the other hand, the screened hybrid xc-functional HSE06 (simply HSE by Heyd, Scuseria, and Ernzerhof) [18,19] developed by mixing nonlocal exact exchange with semilocal exchange correlation is able to provide accurate geometries and formation energies of these compounds [14]. Moreover, HSE is designed to be nonlocal at short range, while the exact exchange is screened at long range. SCAN was demonstrated to capture medium-range weak interactions, while HSE is known to reduce the delocalization error in semilocal functionals. Inspired by these facts, we aim to climb even higher on the rungs of Jacob's ladder to gain more understanding about any competition between weak interactions and free electronlike bonding in Cu-Au systems [20].

In this work, we have revisited the Au-Cu alloy systems using the random phase approximation (RPA) [21–23]. RPA is the simplest approximation within an adiabatic-connection fluctuation-dissipation theorem (ACFDT) formalism [24,25]. It combines the nonlocal one-electron self-interaction free-exact-exchange (EXX) energy with the nonlocal correlation energy ($E_c^{\mathrm{RPA}}$) [26,27]. Most importantly, it can provide accurate results for systems involving weak interactions such as van der Waals (vdW) interactions [28–30], as well as ionic [20,31] and covalent interactions [20,32–34]. The total energy in the ACFDT-DFT framework can be expressed as

$$E = E_{EXX} + E_C^{\mathrm{RPA}}, \tag{1}$$

where $E_{EXX}$ is the Hartree-Fock (HF) total energy evaluated non-self-consistently using self-consistently obtained Kohn-Sham DFT orbitals. $E_C^{\mathrm{RPA}}$ is the RPA correlation energy, which can be obtained using the interacting density-density response function ($\chi$), which is related to the noninteracting response function ($\chi_0$) via a Dyson-like equation [26,27,35]. The RPA correlation energy naturally incorporates long-range dispersion and is nonperturbative. For this work, the systems are heavy coinage metals which are largely influenced by dispersion interactions [36–38]. Furthermore, the systems have zero band gap. Due to its nonperturbative nature, RPA can be safely applied to zero-gap systems without divergence [39]. In both aspects, the application of RPA to these systems is justified.

For the sake of comparison, we also have assessed semilocal functionals such as PBE, PBEsol, the revised TPSS (revTPSS) [40,41], and SCAN along with RPA. We also tested the impact of long-range dispersion through the nonlocal revised VV10 (rVV10) correction by Vydrov and Van Voorhis [42]. We utilized PBE+rVV10 [43,44] and SCAN+rVV10 [45] to check whether the discrepancies in semilocal DFT are due to the absence of long-range dispersion interactions. The rest of the paper is organized as follows. Computational details are provided in Sec. II, followed by results in Sec. III. We will present our conclusions in Sec. IV.

## II. COMPUTATIONAL DETAILS

All DFT calculations were carried out using a projector augmented wave (PAW) [46] method, as implemented in GPAW [47–49] and VASP [50]. We utilized VASP to perform semilocal calculations, whereas RPA calculations were carried out using GPAW. Moreover, semilocal calculations were performed self-consistently, while RPA calculations were carried out using a non-self-consistent approach. We used a plane-wave cutoff of 600 eV and Brillouin zone sampling of $20 \times 20 \times 20$ Gamma centered $k$ mesh to avoid the convergence test for semilocal DFT calculations. Ground-state PBE calculations were performed as an input for the RPA calculations. Separate convergence tests for EXX and the RPA correlation energies were carried out to determine the plane-wave cutoffs and $k$-mesh sampling with less than 2 meV relative error (see Supplemental Material, Table S1 [51]). We used a maximum cutoff of 350 eV to compute the response function. All other parameters and the procedure of the RPA calculations were kept similar to that of Ref. [31], except skipping the gamma point ($\mathbf{q} = 0$) to avoid the possible divergent contribution from metals as discussed in Ref. [32].

We calculated the zero-point vibrational energy (ZPVE) to estimate the thermal contribution to the formation energy. PBEsol [7] calculations were done with a $2 \times 2 \times 2$ supercell (32 atoms) using VASP [52,53] and PHONOPY [54]. The estimated thermal corrections are less than or equal to 1 meV/atom, consistent with previous results [14]. Relativistic effects are included at the scalar level for each atom within the PAW potentials provided in VASP and GPAW. We further tested, at least for PBE and SCAN, an impact of the spin-orbit coupling [55] on semilocal DFT results. We have performed calculations for seven volume points near the experimental equilibrium volume and fit the Birch-Murnaghan equation of state [56] to evaluate the equilibrium properties. We have used the experimental structures from Ref. [17] and varied the lattice constants isotropically to generate structures with different volumes. In order to compute the cohesive energies, atomic energies were computed. We have performed spin-polarized semilocal DFT calculations with VASP using a plane-wave cutoff of 600 eV and $23 \times 24 \times 25$ Å$^3$ simulation cell to avoid any interactions of an isolated atom with its periodic images. Separate convergence tests for atomic energies were performed with GPAW for both EXX and RPA (see Supplemental Material, Table S1 [51]).

## III. RESULTS

### A. Lattice constants

The equilibrium lattice constants of the ordered Au-Cu alloys are presented in Table I. As expected, PBE overestimates the lattice constants and PBEsol yields reasonable lattice constants of the coinage metals such as Au and Cu [20]. The failure of PBE to estimate accurate lattice constants is related to the poor descriptions of exchange-correlation effects between completely filled $d$ shells in coinage metals [20]. RPA lattice constants are also overestimated which can be decreased by including the Pauli repulsion in second-order screened-exchange corrections (SOSEX) or adding a kernel correction to RPA [31,57,58], thereby improving the

TABLE I. Lattice constants (Å). The experimental lattice constants are taken from Ref. [17]. Among the DFT functionals utilized, PBEsol shows the best performance in predicting the equilibrium lattice constant.

| | PBE | PBEsol | revTPSS | SCAN | RPA | Experiment |
|---|---|---|---|---|---|---|
| Cu | 3.64 | 3.57 | 3.57 | 3.57 | 3.63 | 3.62 |
| Au | 4.16 | 4.08 | 4.08 | 4.09 | 4.15 | 4.08 |
| $AuCu_3$ | 3.78 | 3.72 | 3.72 | 3.72 | 3.78 | 3.75 |
| AuCu (fcc) | 3.92 | 3.85 | 3.85 | 3.85 | 3.92 | 3.87 |
| AuCu ($P4/mmm$) | 2.84 | 2.79 | 2.79 | 2.79 | 2.83 | 2.80 |
| $CuAu_3$ | 4.05 | 3.97 | 3.98 | 3.98 | 4.05 | 3.95 |
| MAE (Å) | 0.051 | 0.022 | 0.023 | 0.026 | 0.046 | |
| MAPE (%) | 1.37 | 0.59 | 0.64 | 0.7 | 1.21 | |

short-range correlations necessary to describe the systems with more filled $d$ shells. On the other hand, SCAN along with revTPSS show good performance in the prediction of the equilibrium lattice constant. With the inclusion of kinetic-energy density, both SCAN and revTPSS can distinguish different bonding regions relevant to lattice constants, and this becomes more effective as more $d$ bands are filled in the transition metal [20]. Overall, all methods show a reasonable agreement with the experiment for the lattice constant with mean absolute percentage error (MAPE) less than 1.4%, as shown in Fig. 1. Furthermore, the addition of a long-range dispersion correction slightly improves the PBE lattice constants, while it slightly worsens the SCAN results (see Supplemental Material, Table S2 [51]). The inclusion of spin-orbit coupling can change the PBE and SCAN lattice constants by 1 picometer (see Supplemental Material, Table S3 [51]).

## B. Bulk moduli

The bulk modulus measures the curvature of an energy-volume relation, and its accurate prediction indicates the ability of a DFT approximation to describe the system in a nonequilibrium state with respect to the equilibrium state. We calculated the bulk moduli of various Au-Cu systems and tabulated them in Table II. PBE underestimates the bulk modulus, while PBEsol and revTPSS predict accurate bulk moduli for gold. However, the performance of these functionals worsens on increasing the concentration of copper. On the other hand, SCAN provides an improvement for the bulk modulus of copper, thereby improving the bulk moduli
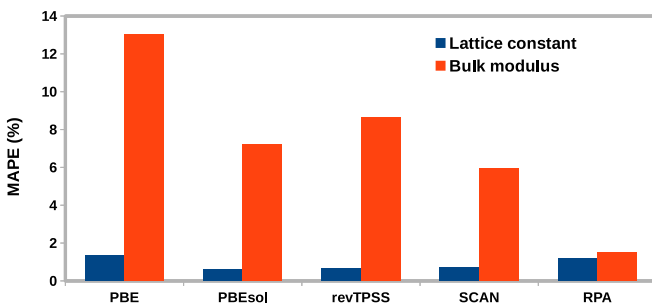


FIG. 1. Mean absolute percentage error (MAPE) for both lattice constants and the bulk moduli. Overall, PBEsol is the most accurate method for lattice constants, while RPA predicts excellent bulk moduli compared to experiments.

of all alloys compared to PBEsol and revTPSS (Fig. 1). The inability of semilocal functionals to give an accurate prediction of bulk moduli indicates their inability to describe the compressed or stretched electron densities with respect to the equilibrium ground-state electron densities. One can see that the overall bulk moduli predicted by PBE for all the alloys are close to the experimental value of copper, while those of other semilocal functionals are closer to gold. On the other hand, RPA provides accurate bulk moduli for both alloys and those of the constituent bulk elemental systems. This indicates that contrary to the lattice constant, the description of short-range correlation is not crucial for the prediction of the bulk modulus. The inclusion of long-range dispersion via rVV10 provides a more significant correction to the bulk modulus for PBE than that for SCAN. On the other hand, spin-orbit coupling (SOC) can increase the bulk moduli by 3–6 GPa with respect to DFT results without SOC (see Supplemental Material, Table S3 [51]).

## C. Formation energy

The formation energy of an Au-Cu alloy can be obtained using

$$\Delta E_f(Au_x Cu_{1-x})$$
$$= \Delta E_{coh}(Au_x Cu_{1-x}) - x\Delta E_{coh}(Au) - (1-x)\Delta E_{coh}(Cu),$$
(2)

where $\Delta E_f(Au_x Cu_{1-x})$, $\Delta E_{coh}(Au_x Cu_{1-x})$, $\Delta E_{coh}(Au)$, and $\Delta E_{coh}(Cu)$ are the formation energy of the system, cohesive energy of the whole system, cohesive energy of gold, and the cohesive energy of copper per atom, respectively, and $x$ is the fraction of gold atoms in the alloys. We have computed the formation energy of a given alloy as a function of crystal volume; see Fig. 2. Experimental volumes are indicated by a "#," whereas the formation energies are represented by black dots. Positive formation energies imply instability of the alloy, while negative formation energies imply stability with respect to their elemental bulk constituents.

Without any correlation, EXX predicts destabilized systems within the range of volumes considered. Contrary to EXX, PBE stabilizes the systems with the presence of both exchange and correlation energies (Fig. 2). Formation energies obtained from PBE agree with RPA values either at the highly compressed state or at the highly stretched state. However, they start to deviate from RPA and even from the experimental value as the equilibrium geometry is approached. On the

TABLE II. Bulk modulus (GPa). Experimental bulk moduli are computed using $\frac{(C_{11}+2C_{12})}{3}$ (cubic lattice), where $C_{ij}$ is the elastic moduli. Overall, RPA predicts the bulk moduli in close agreement with the experiment.

| | PBE | PBEsol | revTPSS | SCAN | HSE [59] | RPA | Experiment |
|---|---|---|---|---|---|---|---|
| Cu | 137.89 | 164.50 | 170.14 | 157.91 | 133.8 | 144.74 | 143.6 [60] |
| Au | 139.03 | 174.34 | 176.01 | 166.95 | 146.6 | 176.71 | 177.6 [61], 180.53 [60] |
| AuCu$_3$ | 139.49 | 168.05 | 171.09 | 164.84 | | 155.25 | 151.83 [62] |
| AuCu (fcc) | 139.99 | 171.02 | 173.12 | 169.47 | | 163.77 | 162.97 [63] |
| AuCu ($P4/mmm$) | 138.75 | 169.56 | 171.90 | 166.16 | | 159.09 | – |
| CuAu$_3$ | 139.03 | 171.64 | 173.25 | 165.74 | | 162.15 | 166.33 [64] |
| MAE (GPa) | 21.71 | 11.04 | 13.19 | 9.31 | | 2.42 | |
| MAPE (%) | 13.02 | 7.20 | 8.65 | 5.93 | | 1.50 | |

contrary, SCAN slightly overbinds the formation energies near the equilibrium geometries, and the overestimation gets larger as we deviate from the equilibrium. The formation energy vs volume calculated with PBEsol and revTPSS behave similarly to that of SCAN; however, they are slightly shifted upward along the direction of positive formation energy. Despite the fact that RPA overestimates the lattice constant, it accurately predicts the curvature and minima of the equation of state for these alloys.

The heats of formation of the Au-Cu system at equilibrium are presented in Table III, whereas the stability of the alloys are represented by a convex hull as in Fig. 3. As in the earlier studies [14,16], PBE severely underestimates the formation

energies. On restoring the second-order gradient expansion for the exchange over a wide range of densities at the GGA level, PBEsol slightly improves the results, but, at the meta-GGA level, revTPSS [40] worsens it. By satisfying more exact constraints and including more appropriate norms [12], SCAN shows a considerable improvement over revTPSS. However, it still performs poorly for copper-rich alloys, while the error decreases on increasing the concentration of gold, as more filled $5d$ shells in Au are involved [20]. The deficiencies in semilocal PBE and SCAN could not be overcome simply by taking thermal correction, long-range dispersion correction, or spin-orbit coupling into account (see Supplemental Material, Tables S2 and S3 [51]). In contrast, nonlocal density
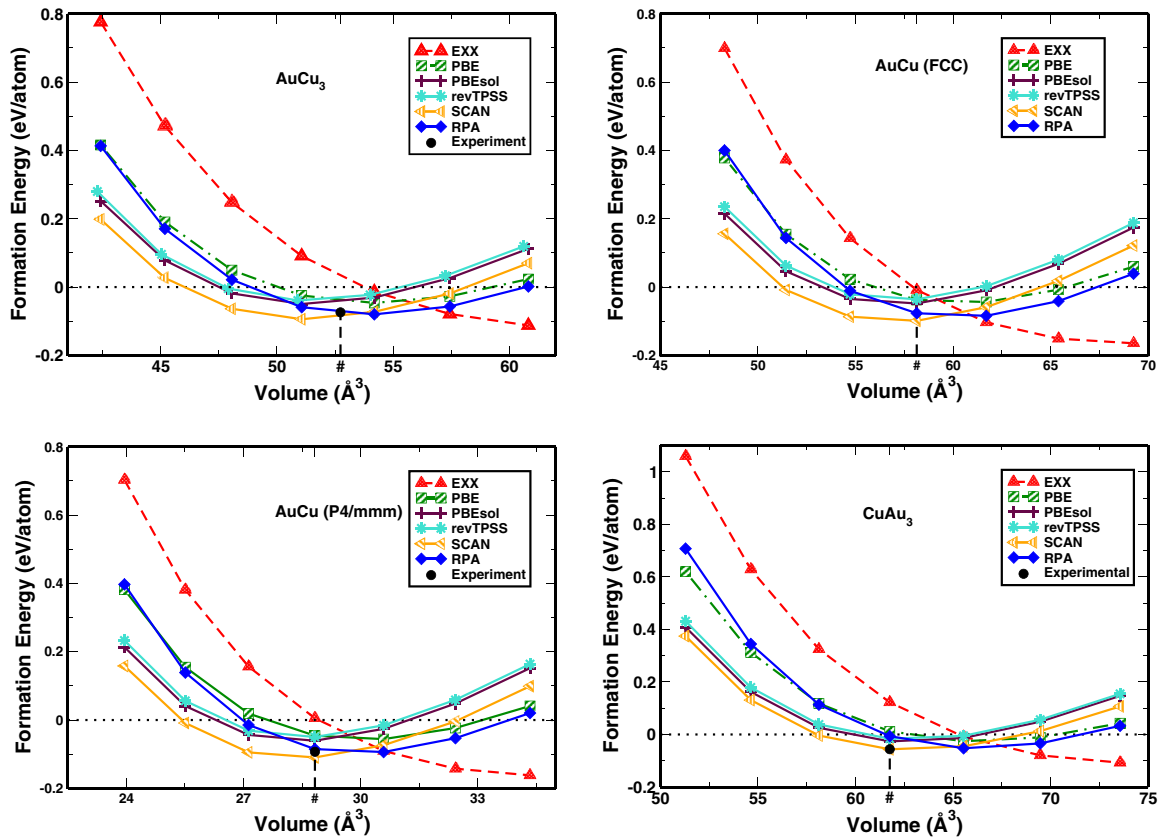


FIG. 2. Formation energy (eV) vs volume (Å$^3$). The positive formation energy refers to the instability of alloys with respect to isolated bulk constituents, while negative formation energy refers to stability. Experimental formation energies are taken from Refs. [1,2]. The experimental volumes are indicated by "#."

TABLE III. The heat of formation (eV/atom). Note that the results for semilocal functionals and HSE are obtained self-consistently, while the RPA results are obtained non-self-consistently using PBE orbitals. Experimental results taken from Ref. [1] are obtained at 320 K, whereas Ref. [2] corresponds to 298.15 K. CuAu$_3$: The experimental structure taken in Ref. [1] is not a fully ordered structure. The heat of formation for a fully ordered CuAu$_3$ is estimated using cubic interpolation of composition (x)-Gibbs energy ($\Delta G$)-entropy ($\Delta S$) of the formation data taken from Ref. [2].

| | PBE | PBEsol | revTPSS | SCAN | HSE [14] | RPA | Experiment [1] |
|---|---|---|---|---|---|---|---|
| AuCu3 | −0.046 | −0.050 | −0.040 | −0.093 | −0.071 | −0.080 | −0.074, −0.075 [2] |
| AuCu (fcc) | −0.047 | −0.050 | −0.037 | −0.101 | | −0.088 | |
| AuCu (P4/mmm) | −0.058 | −0.062 | −0.051 | −0.111 | −0.091 | −0.096 | −0.093 |
| CuAu3 | −0.026 | −0.028 | −0.019 | −0.059 | −0.053 | −0.052 | −0.039, −0.056 [2] |

functionals such as hybrid HSE and RPA consistently predict accurate formation energies of these alloys without any aforementioned corrections. In comparison, self-consistent HSE outperforms non-self-consistent RPA by only a little, but there can be room for improvement when RPA is also evaluated self-consistently [65].

In the present work, both alloys and the constituent metals are in the solid phase and hence possess delocalized electron densities. The reliable prediction of formation energies requires an accurate description of the transition from delocalized electron densities of constituent metals to delocalized electron densities of intermetallic alloys. All semilocal functionals included herein fail to describe such a transition, while the nonlocality present in HSE and RPA is able to effectively detect such changes. However, the transition from localized (atoms) to delocalized (solid metals and alloys) is not straightforward even for nonlocal functionals, as evident from the cohesive energies presented in Table IV. The best density functional for formation energies is the worst for cohesive energies. The hybrid HSE seriously underestimates the cohesive energies of Au-Cu system with a mean absolute error (MAE) of nearly 0.7 eV/atom. Surprisingly, semilocal

functionals perform much better than HSE in the order of PBE < revTPSS < PBEsol < SCAN with decreasing MAE and MAPE. RPA, on the other hand, provides reasonable cohesive energies for Cu-rich compounds, while it worsens on increasing the concentration of gold in the alloys. As the number of filled $d$ bands increases, the short-range correlation becomes more crucial in describing the interactions within transition metal atoms as well as their alloys. Restoring the exchange-correlation kernel within the RPA can improve the cohesive energies of transition metals up to 0.3 to 0.4 eV [34,66].

The performance of various density functionals on Au-Cu alloys clearly depends on their ability to describe the less-delocalized "3$d$" electron density of copper as well as the more-delocalized "5$d$" electron density of gold. SCAN along with PBEsol and revTPSS can effectively describe the 5$d$ bands of gold, thereby giving sensibly accurate lattice constants, bulk moduli, and cohesive energies for Au-rich alloys. However, RPA has the opposite trend in that it can provide an accurate prediction for Cu-rich alloys, but falls short when describing Au-rich alloys. On the contrary, HSE fails to provide accurate bulk moduli and cohesive energies for both copper and gold, giving too-low cohesive energies for both Au- and Cu- rich alloys. With that in mind, one can argue that the density functionals that can separately describe the constituents can ultimately describe the weakly bonded alloys.

## IV. CONCLUSIONS

We have explored copper-gold alloys with various levels of approximations within density functional theory, including the state-of-art random phase approximation. It is difficult to find a universal functional which can describe all of the bonding situations. Semilocal functionals can reasonably describe the transition between localized and delocalized electron densities, as manifested in the cohesive energies. On the other hand, the nonlocality present in HSE and RPA can distinguish the transition between two delocalized electron densities, as seen from the formation energies of the alloys. Moreover, the performance of these functionals in describing the weakly bonded Au-Cu system depends on their potential to separately describe less-delocalized and more-delocalized electron densities of copper and gold, respectively. Based on our results, we can conclude that RPA predicts accurate values for diverse properties of binary alloys, generated from metals with completely filled $d$ shells. It has an accuracy of semilocal functionals at the challenging situations, while consistently
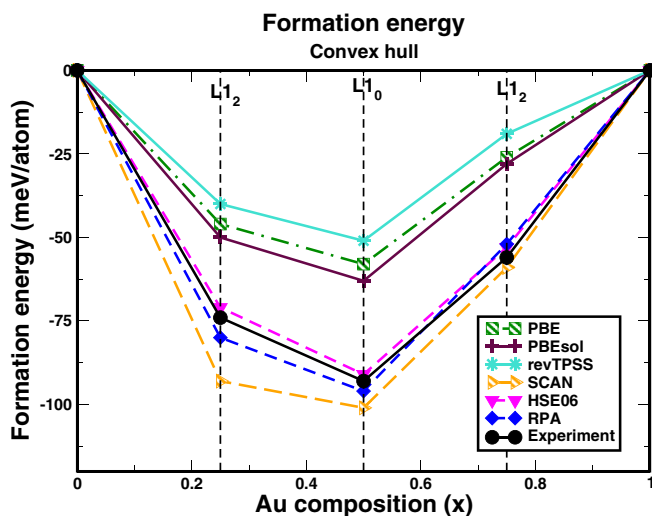


FIG. 3. Convex hull: Formation energy as a function of gold composition (x). PBE along with PBEsol and revTPSS largely underestimates the formation energy, while SCAN performs poorly on a Cu-rich alloy, but improves the result as the concentration of gold increases. Formation energies predicted by nonlocal HSE and RPA are in close agreement with the experiment.

TABLE IV. Cohesive energy per atom (eV/atom). The cohesive energies for HSE are obtained using Refs. [14,59], while the experimental cohesive energies are obtained using Refs. [1,67] using Eq. (2). Among the functionals used, SCAN predicts the most accurate cohesive energy as compared to the experiment.

| | PBE | PBEsol | revTPSS | SCAN | HSE | RPA | Experiment |
|---|---|---|---|---|---|---|---|
| Cu | 3.484 | 4.030 | 4.057 | 3.886 | 3.060 [59] | 3.350 | 3.490 [67] |
| Au | 3.035 | 3.720 | 3.627 | 3.555 | 2.880 [59] | 3.395 | 3.810 [67] |
| AuCu3 | 3.419 | 4.003 | 3.990 | 3.896 | 3.086 | 3.441 | 3.644 |
| AuCu ($P4/mmm$) | 3.317 | 3.937 | 3.893 | 3.828 | 3.111 | 3.469 | 3.743 |
| CuAu3 | 3.175 | 3.826 | 3.753 | 3.695 | 2.978 | 3.436 | 3.786 |
| MAE (eV/atom) | 0.409 | 0.245 | 0.256 | 0.216 | 0.672 | 0.276 | |
| MAPE (%) | 10.84 | 6.78 | 7.08 | 5.93 | 18.05 | 7.41 | |

providing reliable results where semilocal functionals break down.

[1] R. Orr, Acta Metall. **8**, 489 (1960).
[2] R. Hultgren, P. D. Desai, D. T. Hawkins, M. Gleiser, and K. K. Kelley, Selected values of the thermodynamic properties of binary alloys (American Society for Metals, Ohio, 1973).
[3] J. P. Perdew and K. Schmidt, in *Density Functional Theory and Its Applications to Materials*, edited by V. Van Doren, C. Van Alsenoy, and P. Geerlings, AIP Conf. Proc. Vol. 577 (AIP, Melville, NY, 2001), pp. 1–20.
[4] W. Kohn and L. J. Sham, Phys. Rev. **140**, A1133 (1965).
[5] J. P. Perdew, K. Burke, and M. Ernzerhof, Phys. Rev. Lett. **77**, 3865 (1996).
[6] R. Armiento and A. E. Mattsson, Phys. Rev. B **72**, 085108 (2005).
[7] J. P. Perdew, A. Ruzsinszky, G. I. Csonka, O. A. Vydrov, G. E. Scuseria, L. A. Constantin, X. Zhou, and K. Burke, Phys. Rev. Lett. **100**, 136406 (2008).
[8] P. Ziesche, S. Kurth, and J. P. Perdew, Comput. Mater. Sci. **11**, 122 (1998).
[9] J. Tao, J. P. Perdew, V. N. Staroverov, and G. E. Scuseria, Phys. Rev. Lett. **91**, 146401 (2003).
[10] J. Sun, B. Xiao, and A. Ruzsinszky, J. Chem. Phys. **137**, 051101 (2012).
[11] J. Sun, R. Haunschild, B. Xiao, I. W. Bulik, G. E. Scuseria, and J. P. Perdew, J. Chem. Phys. **138**, 044113 (2013).
[12] J. Sun, A. Ruzsinszky, and J. P. Perdew, Phys. Rev. Lett. **115**, 036402 (2015).
[13] E. B. Isaacs and C. Wolverton, Phys. Rev. Mater. **2**, 063801 (2018).
[14] Y. Zhang, G. Kresse, and C. Wolverton, Phys. Rev. Lett. **112**, 075502 (2014).
[15] V. Ozoliņš, C. Wolverton, and A. Zunger, Phys. Rev. B **57**, 6427 (1998).

[16] L.-Y. Tian, H. Levämäki, M. Ropo, K. Kokko, Á. Nagy, and L. Vitos, Phys. Rev. Lett. **117**, 066401 (2016).
[17] H. Okamoto, D. J. Chakrabarti, D. E. Laughlin, and T. B. Massalski, J. Phase Equilib. **8**, 454 (1987).
[18] J. Heyd, G. E. Scuseria, and M. Ernzerhof, J. Chem. Phys. **118**, 8207 (2003).
[19] J. Heyd, G. E. Scuseria, and M. Ernzerhof, J. Chem. Phys. **124**, 219906 (2006).
[20] L. Schimka, R. Gaudoin, J. Klimeš, M. Marsman, and G. Kresse, Phys. Rev. B **87**, 214102 (2013).
[21] D. Bohm and D. Pines, Phys. Rev. **85**, 338 (1952).
[22] D. Bohm and D. Pines, Phys. Rev. **92**, 609 (1953).
[23] D. C. Langreth and J. P. Perdew, Phys. Rev. B **21**, 5469 (1980).
[24] D. C. Langreth and J. P. Perdew, Solid State Commun. **17**, 1425 (1975).
[25] D. C. Langreth and J. P. Perdew, Phys. Rev. B **15**, 2884 (1977).
[26] H. Eshuis, J. E. Bates, and F. Furche, Theor. Chem. Acc. **131**, 1084 (2012).
[27] X. Ren, P. Rinke, C. Joas, and M. Scheffler, J. Mater. Sci. **47**, 7447 (2012).
[28] J. Harl and G. Kresse, Phys. Rev. B **77**, 045136 (2008).
[29] L. Schimka, J. Harl, A. Stroppa, A. Grüneis, M. Marsman, F. Mittendorfer, and G. Kresse, Nat. Mater. **9**, 741 (2010).
[30] S. Lebègue, J. Harl, T. Gould, J. G. Ángyán, G. Kresse, and J. F. Dobson, Phys. Rev. Lett. **105**, 196401 (2010).
[31] N. K. Nepal, A. Ruzsinszky, and J. E. Bates, Phys. Rev. B **97**, 115140 (2018).
[32] J. Harl, L. Schimka, and G. Kresse, Phys. Rev. B **81**, 115126 (2010).
[33] H. Peng and S. Lany, Phys. Rev. B **87**, 174113 (2013).
[34] T. Olsen and K. S. Thygesen, Phys. Rev. B **87**, 075111 (2013).
[35] F. Furche, Phys. Rev. B **64**, 195120 (2001).

[36] C. L. Bracey, P. R. Ellis, and G. J. Hutchings, Chem. Soc. Rev. **38**, 2231 (2009).

[37] J. Mahanty and R. Taylor, Phys. Rev. B **17**, 554 (1978).

[38] A. L. Fetter and J. D. Walecka, *Quantum Theory of Many-particle Systems* (Dover Publications, New York, 2012).

[39] N. Colonna, M. Hellgren, and S. de Gironcoli, Phys. Rev. B **90**, 125150 (2014).

[40] J. P. Perdew, A. Ruzsinszky, G. I. Csonka, L. A. Constantin, and J. Sun, Phys. Rev. Lett. **103**, 026403 (2009).

[41] J. Sun, M. Marsman, G. I. Csonka, A. Ruzsinszky, P. Hao, Y.-S. Kim, G. Kresse, and J. P. Perdew, Phys. Rev. B **84**, 035117 (2011).

[42] O. A. Vydrov and T. Van Voorhis, J. Chem. Phys. **133**, 244103 (2010).

[43] H. Peng and J. P. Perdew, Phys. Rev. B **95**, 081105(R) (2017).

[44] S. Adhikari, H. Tang, B. Neupane, G. I. Csonka, and A. Ruzsinszky, arXiv:1906.01091.

[45] H. Peng, Z.-H. Yang, J. P. Perdew, and J. Sun, Phys. Rev. X **6**, 041005 (2016).

[46] P. E. Blöchl, Phys. Rev. B **50**, 17953 (1994).

[47] M. Walter, H. Häkkinen, L. Lehtovaara, M. Puska, J. Enkovaara, C. Rostgaard, and J. J. Mortensen, J. Chem. Phys. **128**, 244101 (2008).

[48] J. J. Mortensen, L. B. Hansen, and K. W. Jacobsen, Phys. Rev. B **71**, 035109 (2005).

[49] S. R. Bahn and K. W. Jacobsen, Comput. Sci. Eng. **4**, 56 (2002).

[50] J. Hafner, J. Comput. Chem. **29**, 2044 (2008).

[51] See Supplemental Material at http://link.aps.org/supplemental/10.1103/PhysRevB.100.045135 for files containing energy-volume data, a PYTHON script, and information about the data and convergence tests referenced in the manuscript.

[52] G. Kresse and J. Furthmüller, Phys. Rev. B **54**, 11169 (1996).

[53] G. Kresse and D. Joubert, Phys. Rev. B **59**, 1758 (1999).

[54] A. Togo and I. Tanaka, Scr. Mater. **108**, 1 (2015).

[55] S. Steiner, S. Khmelevskyi, M. Marsmann, and G. Kresse, Phys. Rev. B **93**, 224425 (2016).

[56] F. Birch, Phys. Rev. **71**, 809 (1947).

[57] J. E. Bates, S. Laricchia, and A. Ruzsinszky, Phys. Rev. B **93**, 045119 (2016).

[58] A. Grüneis, M. Marsman, J. Harl, L. Schimka, and G. Kresse, J. Chem. Phys. **131**, 154115 (2009).

[59] P. Janthon, S. Luo, S. M. Kozlov, F. Vines, J. Limtrakul, D. G. Truhlar, and F. Illas, J. Chem. Theory Comput. **10**, 3832 (2014).

[60] H. B. Huntington, in *Solid State Physics* (Elsevier, New York, 1958), Vol. 7, pp. 213–351.

[61] F. Cardarelli, in *Materials Handbook: A Concise Desktop Reference* (Springer International, Cham, 2018), pp. 317–695.

[62] S. G. O'Hara and B. J. Marshall, Phys. Rev. B **3**, 4002 (1971).

[63] C. Teodosiu, *Elastic Models of Crystal Defects* (Springer, Berlin, Heidelberg, 2013).

[64] G. Simmons and H. Wang, *Single Crystal Elastic Constants and Calculated Aggregate Properties: A Handbook 2nd Edition* (MIT Press, Cambridge, MA, 1991).

[65] N. L. Nguyen, N. Colonna, and S. de Gironcoli, Phys. Rev. B **90**, 045138 (2014).

[66] T. S. Jauho, T. Olsen, T. Bligaard, and K. S. Thygesen, Phys. Rev. B **92**, 115140 (2015).

[67] C. Kittel, P. McEuen, and P. McEuen, *Introduction to Solid State Physics* (Wiley, New York, 1976), Vol. 8.